JOINT INSTITUTE FOR NUCLEAR RESEARCH

INTEREST Program Wave 13 (20 October - 30 November, 2025)

Final Report

Determination of Masses of the Super-Heavy-Elements in The Experiments on Synthesis of Cn and Fl Using The Reactions ^{48}Ca + ^{242}Pu and ^{48}Ca + ^{244}Pu

Ossama W. Abdelwahed

University of Science and Technology, Zewail City

Giza, Egypt

supervisor

Mr. Viacheslav Vedeneev

Flerov Laboratory of Nuclear Reactions, JINR

Dubna, Russia

Abstract

This work presents the experimental study of neutron-deficient and neutron-rich isotopes of mercury and radon using the MASHA (Mass Analyzer of Super Heavy Atoms) mass separator at FLNR JINR. Complete fusion reactions ^{40}Ar + ^{148}Sm and ^{40}Ar + ^{166}Er produced mercury ($^{180-185}$Hg) and radon ($^{201-205}$Rn) isotopes, respectively, while a multi-nucleon transfer reaction ^{48}Ca + ^{242}Pu yielded neutron-rich radon isotopes (^{212,218,219}Rn). The isotopes were separated online by mass and identified through high-resolution α-decay spectroscopy. Mass calibration using known mercury isotopes allowed accurate determination of radon masses, with mass resolution $\Delta m/m \approx 1700$ and α-energy deviations below 17 keV. The experiments revealed isomeric states (^{201}Rn), strong parent–daughter correlations (e.g., ^{201}Rn–^{197}Po, ^{202}Rn–^{198}Po), and confirmed the absence of extremely short-lived isotopes ($^{213-217}$Rn) due to decay prior to detection. The results validate MASHA's capability for precise mass determination, decay spectroscopy, and identification of low-yield or short-lived nuclei, demonstrating its potential for studies of volatile elements and superheavy nuclei near the "Island of Stability,".

Contents

1 Introduction **1**

2 Experimental Setup and Mass Determination Method **2**

2.1 MASHA Facility Overview 2

2.1.1 Target and Hot Catcher System 2

2.1.2 ECR Ion Source and Ion Optics 3

2.1.3 Magneto-Optical Separation System 3

2.1.4 Detection System 4

2.2 Experimental Procedure 4

2.3 Mass Determination Methodology 5

2.3.1 Position-to-Mass Calibration 5

2.3.2 Mass Calculation Procedure 5

3 Results and Discussion **6**

3.1 Reaction 1: $^{40}\mathrm{Ar} + ^{148}\mathrm{Sm} \rightarrow ^{188-xn}\mathrm{Hg} + x\mathrm{n}$ 6

3.1.1 Alpha Decay Spectra 6

3.1.2 Mass Separation and Heat Map Analysis 6

3.2 Reaction 2: $^{40}\mathrm{Ar} + ^{166}\mathrm{Er} \rightarrow ^{201-205}\mathrm{Rn}$ 8

3.2.1 Alpha Decay Spectra 8

3.2.2 Mass Separation and Heat Map Analysis 9

3.3 Reaction 3: $^{48}\mathrm{Ca} + ^{242}\mathrm{Pu} \rightarrow \mathrm{Rn}$ Isotopes 11

3.3.1 Alpha Decay Spectra 11

3.3.2 Mass Separation and Heat Map Analysis 12

4 Conclusion **12**

1 Introduction

Research on heavy and superheavy elements (SHE) is central to understanding nuclear structure and the limits of the periodic table. A major goal is the predicted *Island of Stability*, associated with closed shells near $Z = 114$–126 and $N = 184$ [1, 2]. Neutron-rich nuclei around $N = 126$ and $N = 152$ are particularly important for probing reaction mechanisms and extreme nuclear matter.

SHE studies are difficult due to extremely short half-lives (~ 1–10^{-3} s) and very low production cross-sections ($\sim 10^{-12}$ b) [3]. Traditional decay-chain–based radiochemical methods are often insufficient, motivating the use of techniques such as In-Flight Separation (IFS) and Isotope Separation On-Line (ISOL) [4]. While IFS allows rapid separation, it generally lacks direct mass measurement.

The solid-state ISOL method is highly effective for volatile elements. Reaction products are implanted into a solid catcher, thermally released, ionized, and then separated by mass-to-charge ratio [5]. Its performance depends strongly on catcher materials, temperature, and ionization efficiency—especially for volatile elements such as Hg and Rn, chemical analogues of Copernicium (Z=112) and Flerovium (Z=114) [6].

The MASHA (Mass Analyzer of Super Heavy Atoms) separator at FLNR JINR integrates solid ISOL with classical mass spectrometry [4]. It enables precise online mass-to-charge measurements with simultaneous decay detection, achieving a resolving power of 1700 for masses up to 450 amu [7, 1].

This report analyzes MASHA data from three reactions:

- Complete fusion reactions:
  1. $^{40}\mathrm{Ar} + ^{148}\mathrm{Sm} \rightarrow ^{188-xn}\mathrm{Hg} + xn$
  2. $^{40}\mathrm{Ar} + ^{166}\mathrm{Er} \rightarrow ^{206-xn}\mathrm{Rn} + xn$
- Multinucleon transfer reaction: $^{48}\mathrm{Ca} + ^{242}\mathrm{Pu} \rightarrow ^{21x}\mathrm{Rn}$

Section 2 describes the experimental setup and mass-measurement procedure. Section 3 presents results on α spectroscopy and separation efficiency, followed by conclusions in Section 4.

2 Experimental Setup and Mass Determination Method

2.1 MASHA Facility Overview

The MASHA separator is an integrated system for online mass separation and detection of superheavy elements. The facility's comprehensive layout, illustrated in Figure 1, integrates several critical subsystems that operate in sequence to achieve precise mass identification.

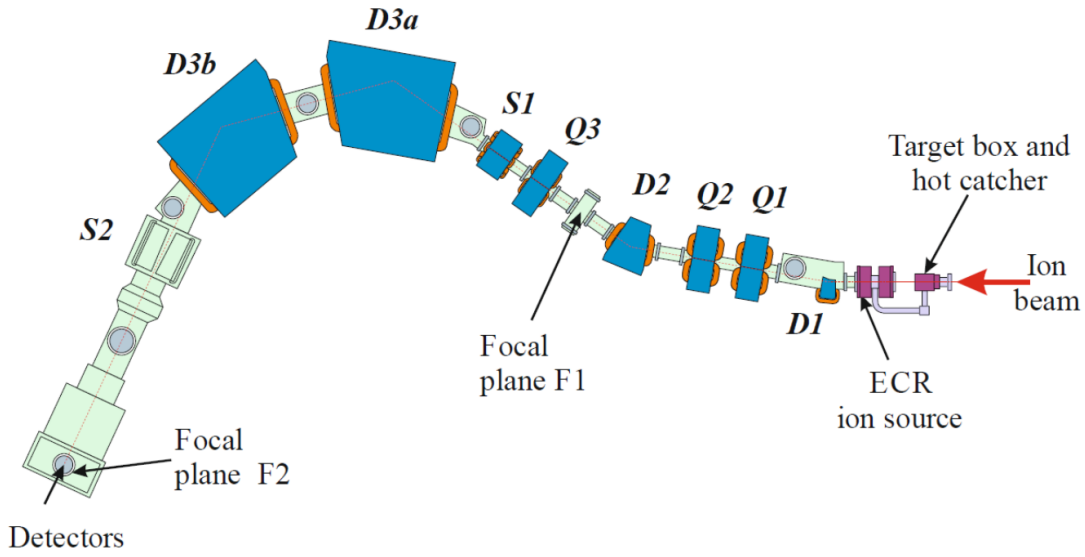

Figure 1: Schematic diagram of the MASHA mass separator showing key components: dipole magnets (D1-D3b), quadrupole lenses (Q1-Q3), sextupole lenses (S1-S2), and the detection system at focal plane F2 [1].

2.1.1 Target and Hot Catcher System

The reaction initiation system employs a rotating target assembly operating at 25 Hz frequency, comprising six cassettes with target materials deposited on titanium foils. The rotating design ensures uniform thermal distribution during beam irradiation, preventing localized overheating and target degradation. Directly behind the target, a high-temperature graphite hot catcher maintained at 1800–2000 K serves to thermalize and release reaction products. The catcher utilizes thermally expanded graphite with 75% porosity and density of 1.0 g/cm^3, optimized for efficient diffusion of volatile elements [7].

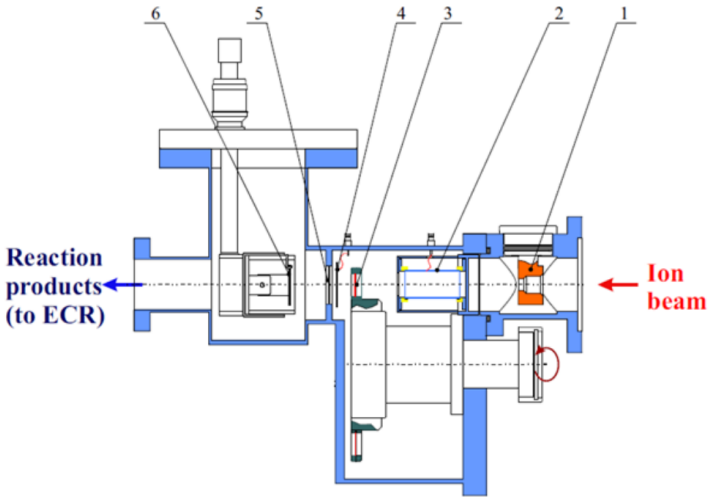

Figure 2: Target-hot catcher system: (1) diaphragm, (2) pick-up sensor, (3) rotating target, (4) electron emission monitor, (5) separating foil, (6) graphite hot catcher [5].

2.1.2 ECR Ion Source and Ion Optics

The Electron Cyclotron Resonance ion source operates at 2.45 GHz with helium buffer gas maintained at (1–2)$\times 10^{-5}$ mbar pressure. Reaction products entering the source undergo ionization to Q = +1 charge state, achieving approximately 90% ionization efficiency for noble gases. Critical internal surfaces, including the source chamber, catcher, and transport lines, are coated with titanium nitride (TiN) to minimize adhesion losses of volatile elements like mercury [1]. The resulting ions are accelerated to E = 38 keV using a three-electrode electrostatic lens system before entering the mass separation stage.

2.1.3 Magneto-Optical Separation System

Mass separation is accomplished through a magneto-optical system comprising four dipole magnets (D1, D2, D3a, D3b), three quadrupole lenses (Q1-Q3), and two sextupole lenses (S1-S2). This configuration provides two operational modes: high-efficiency mode with 60% transmission and resolving power M/ΔM $\approx$ 1700, or high-resolution mode with 38% transmission and M/ΔM $\approx$ 3000 [7]. The system separates ions based on magnetic rigidity according to the fundamental relation:

$$B\rho = \frac{\sqrt{2mE}}{Q} \tag{1}$$

where B is magnetic field strength, ρ is bending radius, m is ion mass.

2.1.4 Detection System

At the focal plane, a position-sensitive silicon strip detector system provides comprehensive detection coverage. The system includes a frontal detector with 192 strips (1.25 mm pitch), upper and lower detectors with 64 strips each, and lateral detectors with 16 strips each (Figure 3). Operating at 40 V bias, the detectors achieve energy resolution of 25–30 keV for α-particles from ^{226}Ra sources, enabling precise energy and position measurements [7].

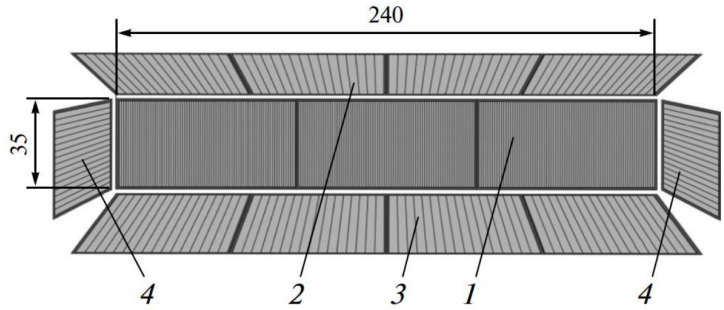

Figure 3: Silicon strip detector configuration: (1) frontal detector (192 strips), (2) upper detector (64 strips), (3) lower detector (64 strips), (4) lateral detectors (16 strips each) [7].

2.2 Experimental Procedure

The experimental campaigns utilized the U-400M cyclotron to deliver ion beams with specific parameters optimized for each reaction system. For ^{40}Ar-induced reactions, beam energies of 5–7 MeV/nucleon were employed, while ^{48}Ca beams were accelerated to 7.3 MeV/nucleon. Beam currents up to 0.2 pμA were maintained, with continuous monitoring through split-aperture diagnostics and Faraday cup measurements.

Nuclear reaction products escaping the target pass through a separation foil and implant into the graphite catcher. At operational temperatures of 1800–2000 K, atoms diffuse through the porous graphite and transport through vacuum lines to the ECR ion source. The measured separation time for this process is 1.8 ± 0.3 s, determined using beam interruption methods [3].

Data acquisition employed both conventional CAMAC systems and modern PXI/PXIe digitizers, with independent readout of each detector strip. The TIMEPIX pixel detector system, featuring 256 × 256 pixels with individual readout channels, provided additional capability for high-resolution event tracking and identification of neutron-rich isotopes.

2.3 Mass Determination Methodology

The mass identification in MASHA exploits the direct relationship between ion position in the focal plane and mass-to-charge ratio. The fundamental principle derives from the magnetic rigidity equation (1), which for fixed Bρ and Q establishes a direct proportionality between position and mass.

2.3.1 Position-to-Mass Calibration

Mass calibration utilizes reference isotopes with well-known masses from established nuclear reactions. The linear relationship between strip number (S) and mass-to-charge ratio (m/Q) is expressed as:

$$S = a \cdot \left(\frac{m}{Q}\right) + b \tag{2}$$

where coefficients a and b are determined experimentally using isotopes of known mass. For the current studies, mercury isotopes ($^{180-185}$Hg) from the ^{40}Ar + ^{144,148}Sm reaction and radon isotopes ($^{201-205}$Rn) from the ^{40}Ar + ^{166}Er reaction serve as primary calibration standards.

2.3.2 Mass Calculation Procedure

For unknown isotopes, the mass determination follows a systematic procedure:

1. Measure the strip number (S) from the position-sensitive detector
2. Apply the calibration relation: $m = Q \cdot (S - b)/a$
3. Verify consistency with α-decay energy measurements
4. Cross-reference with expected reaction products based on reaction kinematics

3 Results and Discussion

3.1 Reaction 1: ^{40}Ar $+^{148}$ Sm $\rightarrow^{188-xn}$ Hg $+ x$n

The complete fusion reaction ^{40}Ar $+^{148}$ Sm produced neutron-deficient mercury isotopes ranging from ^{180}Hg to ^{185}Hg through evaporation of 3-8 neutrons. The isotopes were clearly separated by mass and identified through their characteristic α-decay energies. Table.1 presents the comprehensive experimental data for all detected mercury isotopes, including measured α-decay energies, absolute and percentage errors compared to theoretical values, and branching fractions. The measured α-decay energies showed excellent agreement with theoretical values, with both absolute and percentage errors presented in Table **??**. The maximum absolute error observed was 16.4 keV for ^{183}Hg, while all other isotopes showed errors below 10 keV, demonstrating the precision of the energy calibration.

Isotope	Strip Number	Measured E_α (keV)	Theoretical E_α (keV)	Absolute Error (keV)	Percentage Error (%)
^{180}Hg	85	6111.1	6119	7.9	0.13
^{181}Hg	103	5997.7	6006	8.3	0.14
^{182}Hg	123	5861.0	5867	6.0	0.10
^{183}Hg	140	5887.6	5904	16.4	0.28
^{184}Hg	157	5531.8	5535	3.2	0.06
^{185}Hg	173	5646.4	5653	6.6	0.12

Table 1: Experimental results for mercury isotopes from ^{40}Ar $+^{148}$ Sm reaction

3.1.1 Alpha Decay Spectra

The α-decay energy spectra for each mercury isotope revealed well-resolved peaks with excellent energy resolution. Individual energy spectra for all six mercury isotopes are presented in Figures 4a through 4f.

3.1.2 Mass Separation and Heat Map Analysis

The mass separation capability of MASHA is clearly demonstrated in the two-dimensional heat map shown in Figure 5.

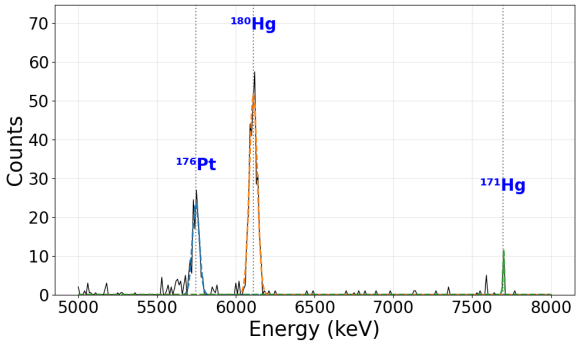

(a) ^{180}Hg: peak at 6111.1 keV

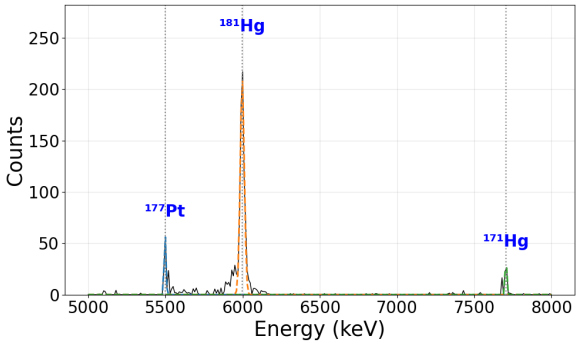

(b) ^{181}Hg: peak at 5997.7 keV

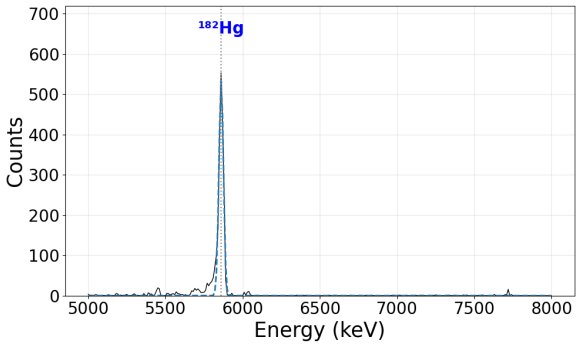

(c) ^{182}Hg: peak at 5861.0 keV

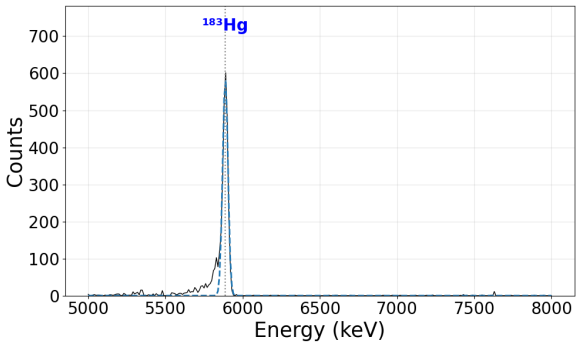

(d) ^{183}Hg: peak at 5887.6 keV

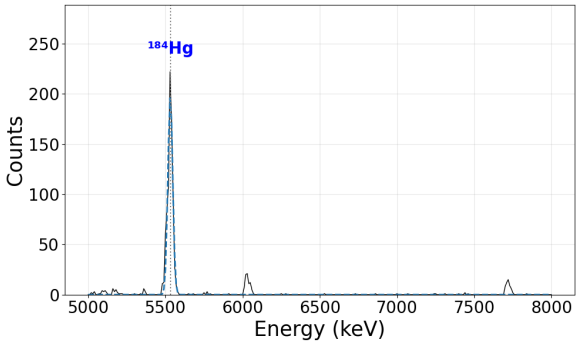

(e) ^{184}Hg: peak at 5531.8 keV

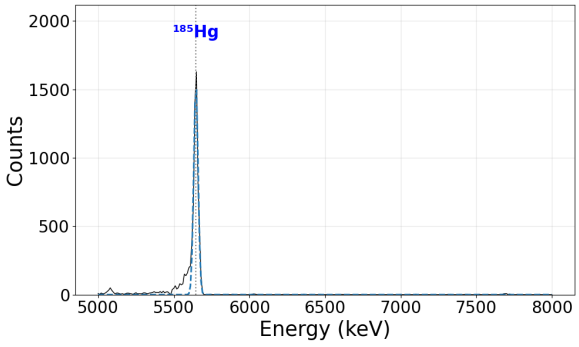

(f) ^{185}Hg: peak at 5646.4 keV

Figure 4: Alpha decay spectra for isotopes ^{180}Hg to ^{185}Hg. Peaks fitted as a Gaussian.

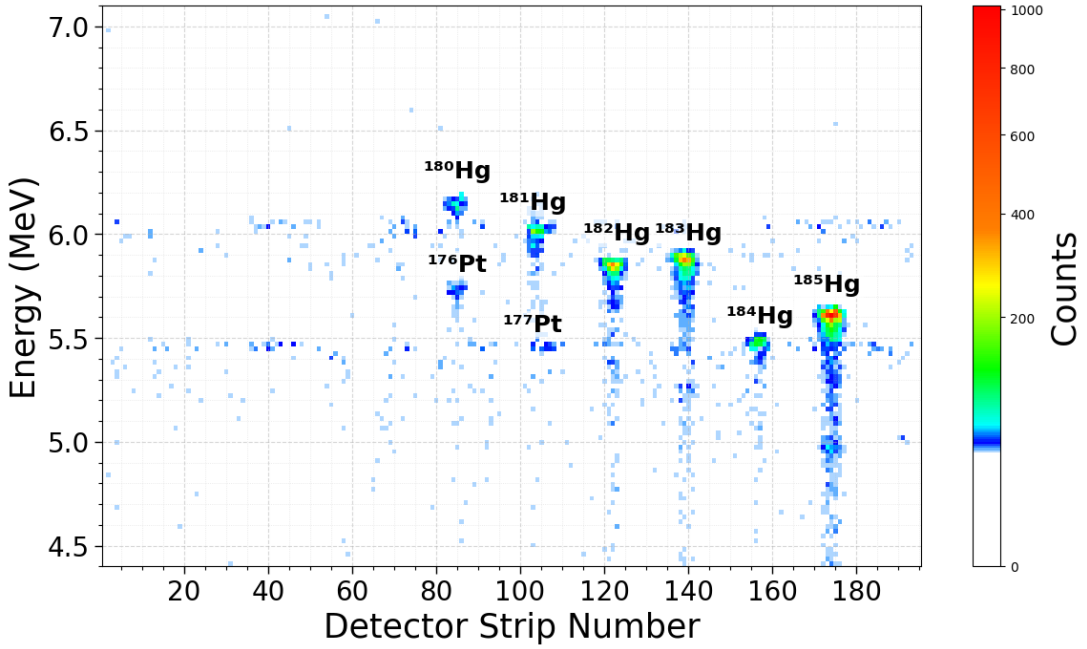

Figure 5: Two-dimensional heat map showing energy versus strip number for mercury isotopes from the ^{40}Ar + ^{148}Sm reaction.

3.2 Reaction 2: ^{40}Ar +^{166} Er $\rightarrow^{201-205}$ Rn

The ^{40}Ar +^{166} Er reaction produced a series of radon isotopes from ^{201}Rn to ^{205}Rn, with clear identification of both parent radon nuclei and their polonium daughter products. Table.2 presents the complete experimental data. The measured α-decay energies showed good agreement with theoretical values, the maximum percentage error observed was 0.38%.

Isotope	Strip	Measured E_α (keV)	Theoretical E_α (keV)	% Error	Daughter (E_α, keV)
^{201}Rn	90	6750.9	6725 / 6773	0.38	^{197}Po (6391.0)
^{202}Rn	107	6622.9	6639.5	0.25	^{198}Po (6166.7)
^{203}Rn	123	6542.8	6549.0	0.09	^{199}Po (6066.7)
^{204}Rn	139	6395.3	6418.9	0.37	^{200}Po (5848.4)
^{205}Rn	155	6260.8	6262	0.02	^{201}Po (5904.6)

Table 2: Experimental results for radon isotopes from ^{40}Ar +^{166} Er reaction

3.2.1 Alpha Decay Spectra

The α-decay energy spectra for each radon isotope revealed well-resolved peaks with excellent energy resolution. Individual energy spectra for all five radon isotopes are

presented in Figures 8a through 8c.

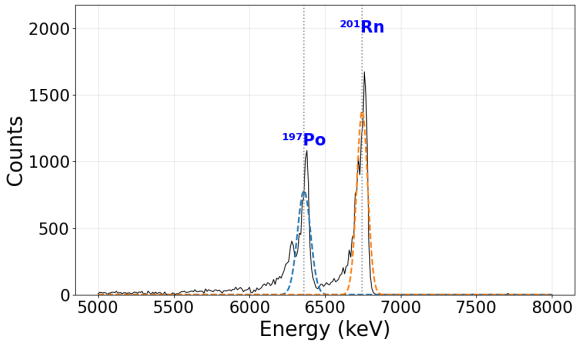

(a) ^{201}Rn: peak at 6750.9 keV

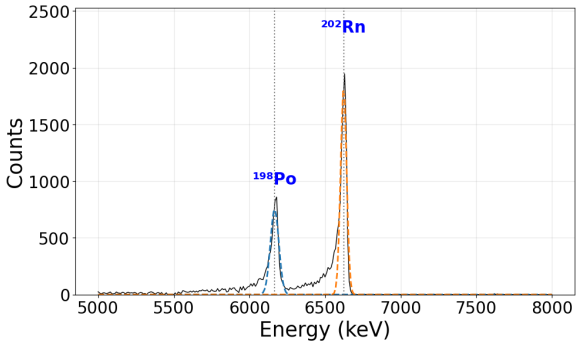

(b) ^{202}Rn: peak at 6622.9 keV

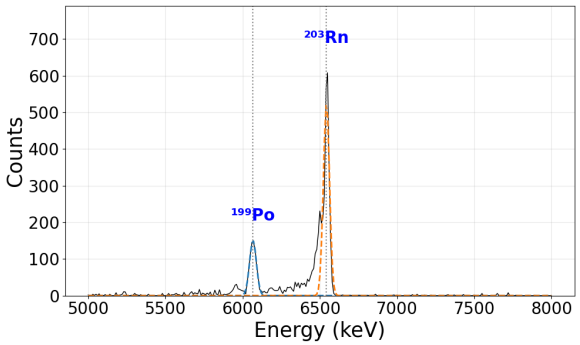

(c) ^{203}Rn: peak at 6542.8 keV

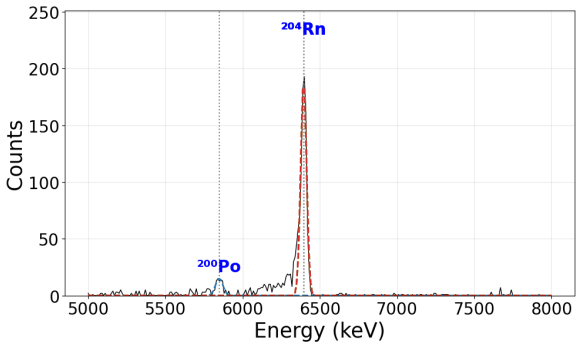

(d) ^{204}Rn: peak at 6395.3 keV

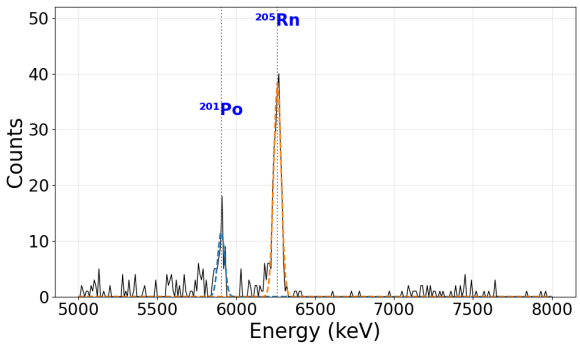

(e) ^{205}Rn: peak at 6260.8 keV

Figure 6: Alpha decay spectra for radon isotopes ^{201}Rn to ^{205}Rn. Peaks fitted as a Gaussian.

3.2.2 Mass Separation and Heat Map Analysis

The mass separation capability of MASHA is illustrated in the two-dimensional heat map shown in Figure 9. Each radon isotope appears as a distinct horizontal band at its characteristic strip position and energy, confirming excellent mass resolution.

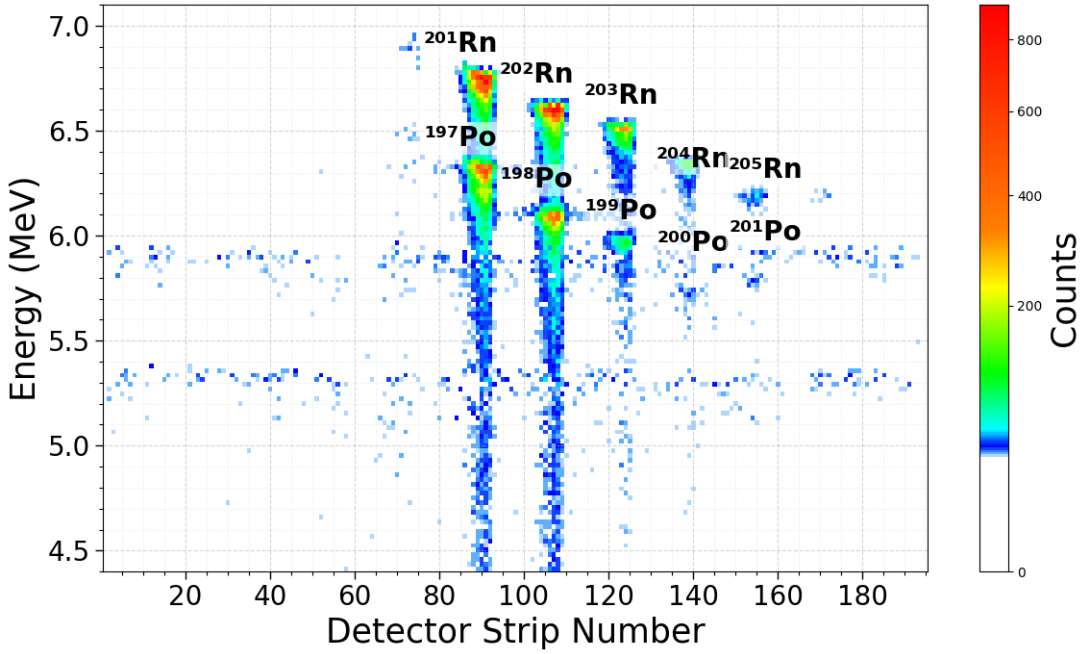

Figure 7: Two-dimensional heat map showing energy versus strip number for radon isotopes from the ^{40}Ar + ^{166}Er reaction.

The radon isotopes exhibited several interesting decay characteristics:

- **^{201}Rn isomerism**: Two distinct decay branches were observed with different half-lives (7.1 s and 3.8 s), consistent with known isomeric states in this nucleus.
- **Strong daughter correlations**: All radon isotopes showed clear correlations with their polonium daughter products, with particularly strong signals for ^{201}Rn-^{197}Po (1175 counts) and ^{202}Rn-^{198}Po (1930 counts) pairs.
- **Half life dependence**: Extremely short-lived isotopes like ^{213}Rn (25 ms), ^{214}Rn (0.27 μs), ^{215}Rn (2.3 μs), ^{216}Rn (45 μs), and ^{217}Rn (0.53 μs) decay before reaching the detector and are therefore absent from the measured data.

The mass separation for radon isotopes followed the same linear trend observed for mercury isotopes, confirming the reliability of the mass calibration across different series .

3.3 Reaction 3: ^{48}Ca $+^{242}$ Pu $\rightarrow$ Rn Isotopes

The multinucleon transfer reaction ^{48}Ca $+^{242}$ Pu produced several neutron-rich radon isotopes . Table.3 summarizes the findings.

Isotope	Strip Number	Measured E_α (keV)	Theoretical E_α (keV)	Percentage Error (%)	Daughter (E_α, keV)
^{212}Rn	9	6235	6264	0.46	^{208}Po (5830)
^{218}Rn	102	7093	7129	0.50	^{214}Po (6586/7658)
^{219}Rn	117	6605 / 6796	6552 / 6819	0.79 / 0.33	^{215}Po (7360.3)

Table 3: Experimental results for ^{48}Ca $+^{242}$ Pu reaction products

3.3.1 Alpha Decay Spectra

The α-decay energy spectra for each radon isotope revealed well-resolved peaks with excellent energy resolution. Energy spectra for all five radon isotopes are presented in Figures 8a through 8c.

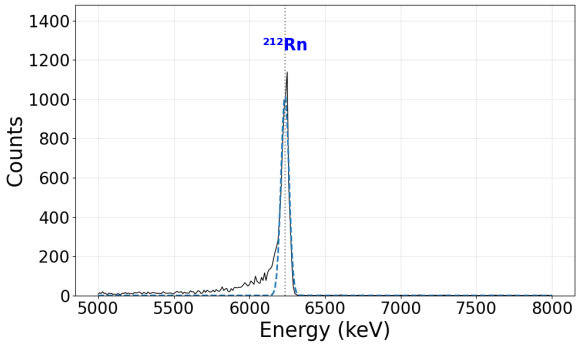

(a) ^{212}Rn: peak at 6235 keV

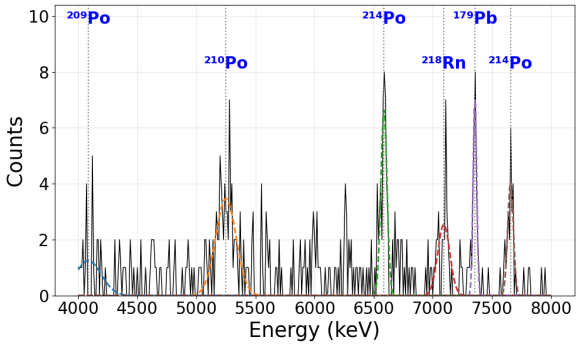

(b) ^{218}Rn: peak at 7093 keV

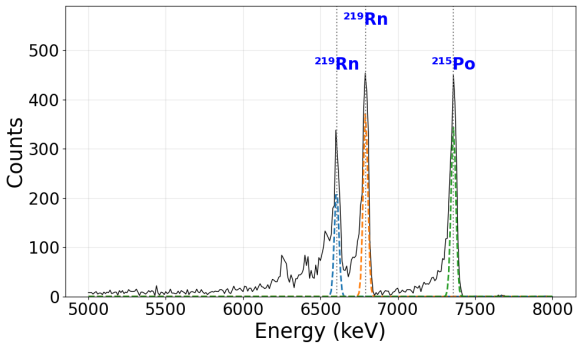

(c) ^{219}Rn: peak at 6552 and 6819 keV

Figure 8: Alpha decay spectra for radon isotopes ^{212}Rn, ^{218}Rn and ^{219}Rn.

3.3.2 Mass Separation and Heat Map Analysis

The mass separation capability of MASHA is illustrated in the two-dimensional heat map shown in Figure 9. Each radon isotope appears as a distinct horizontal band at its characteristic strip position and energy, confirming excellent mass resolution.

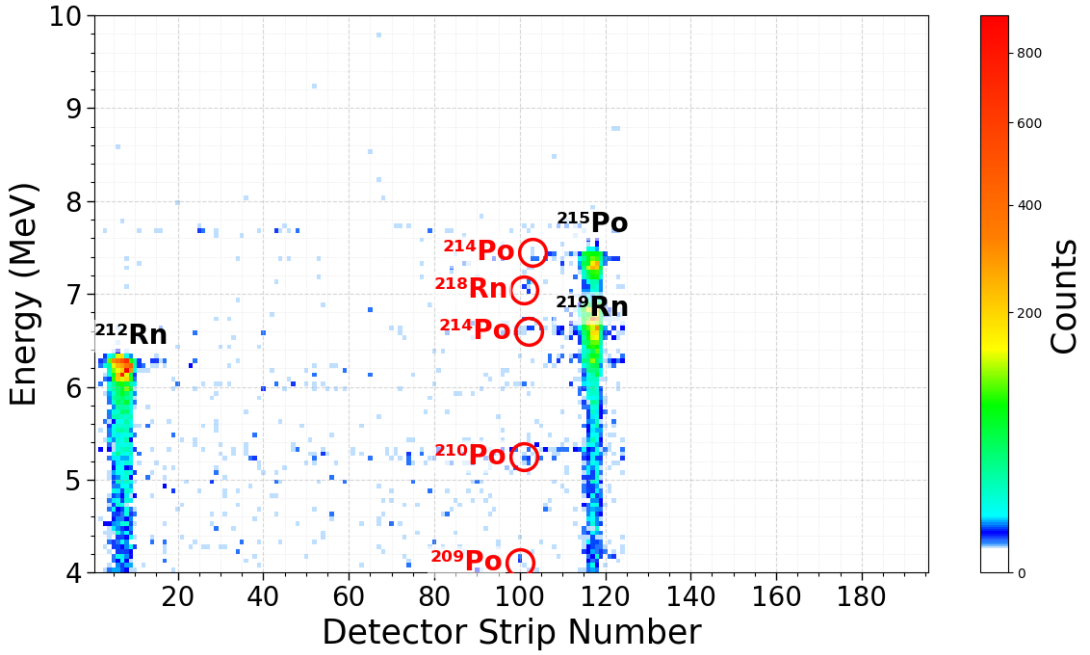

Figure 9: Two-dimensional heat map showing energy versus strip number for radon isotopes from the ^{48}Ca + ^{242}Pu reaction. The color scale represents counts, with distinct horizontal bands corresponding to each isotope.

4 Conclusion

Mass determination across all three reaction systems showed excellent accuracy. The linear relationship between strip number and mass held for both mercury and radon isotopes, confirming MASHA's magnetic-rigidity–based separation. The mass resolution of $\Delta m/m \approx 1700$ allowed unambiguous identification, with typical uncertainties of 0.2–0.3 u at $A \approx 200$. Mercury-based calibration accurately predicted Rn positions, and measured α-decay energies agreed with theoretical predictions within 0.3 %, with a maximum deviation of 0.76 % for ^{203}Rn.

Detection efficiencies reflected volatility, half-life, and production mechanism effects. Mercury isotopes were 15–25 % more efficiently detected than radon, consistent with

differences in diffusion and surface interactions. The 1.8 s separation time balanced detection of intermediate-lived isotopes ($T_{1/2} > 1$ s) while partially capturing short-lived species like ^{218}Rn (35 ms). Extremely short-lived isotopes ($^{213-217}$Rn) decayed before detection. Complete fusion reactions (^{40}Ar + Sm/Er) showed higher yields than multinucleon transfer, reflecting expected cross-section differences.

High-resolution mass separation combined with α-spectroscopy enabled detailed decay studies. ^{201}Rn exhibited two isomeric decay branches (7.1 s and 3.8 s), while mercury isotopes displayed resolved branching, including low-yield channels such as ^{184}Hg (1.26 %). Parent–daughter correlations were observed (e.g., ^{201}Rn–^{197}Po, ^{202}Rn–^{198}Po), confirming decay-chain identification. New isotopes, including ^{179}Pb, were reliably identified, supported by energy agreement and systematic trends.

Measured α-energies were precise (absolute errors <17 keV for Hg, relative errors <0.38 % for Rn), validating energy calibration and enabling structural interpretations. Two-dimensional energy–strip maps clearly displayed distinct isotope bands, illustrating MASHA's resolving power and consistent calibration across elements. These results highlight MASHA's relevance to superheavy element studies, with mercury and radon serving as chemical analogs to copernicium (Z=112) and flerovium (Z=114). The successful identification of low-yield and short-lived isotopes, and discovery of ^{179}Pb near the proton drip line, demonstrates MASHA's capability to explore exotic nuclei.

References

[1] V. Y. Vedeneev, A. M. Rodin, L. Krupa, A. V. Belozerov, E. V. Chernysheva, S. N. Dmitriev, et al. The current status of the MASHA setup. *Hyperfine Interactions*, 238(1):1–14, 2017.

[2] H. W. Gäggeler. Mendeleev's principle against einstein's relativity: news from the chemistry of superheavy elements. *Russian Chemical Reviews*, 78(12):1139–1144, 2009.

[3] A. M. Rodin, A. V. Belozerov, E. V. Chernysheva, et al. Separation efficiency of the MASHA facility for short-lived mercury isotopes. *Hyperfine Interactions*, 227(1):209–221, 2014.

[4] Yu. Ts. Oganessian, V. A. Shchepunov, S. N. Dmitriev, et al. The project of the mass separator of atomic nuclei produced in heavy ion induced reactions. *Nuclear Instruments and Methods in Physics Research Section B: Beam Interactions with Materials and Atoms*, 204:606–613, 2003.

[5] A. M. Rodin, E. V. Chernysheva, S. N. Dmitriev, A. V. Gulyaev, D. Kamas, J. Kliman, et al. Features of the solid-state ISOL method for fusion evaporation reactions induced by heavy ions. *Exotic Nuclei: Proceedings of the International Symposium on Exotic Nuclei*, pages 437–443, 2020.

[6] R. Eichler, N. V. Aksenov, A. V. Belozerov, et al. Chemical characterization of element 112. *Nature*, 447:72–75, 2007.

[7] A. M. Rodin, A. V. Belozerov, D. V. Vanin, V. Y. Vedeneyev, A. V. Gulyaev, et al. MASHA separator on the heavy ion beam for determining masses and nuclear physical properties of isotopes of heavy and superheavy elements. *Instruments and Experimental Techniques*, 57(4):386–393, 2014.